Ultra-Wideband Planar Dipole Array Antenna for Multifunction Phased Array Radars

Bin Li[1, 2, *], Zhipeng Zhou[1, 2], and Lei Sun[1, 2]

Abstract—In the study, an ultra-wideband array antenna for multifunction phased array radars (MPAR) is proposed. Due to the low-profile and ultra-wideband characteristics, the planar dipole elements are utilized to form an array antenna. Their performances are enhanced by using an optimized microstrip-sector feeding structure. The array antenna is a combination of subarrays, each of which corresponds to 4×4 transmit/receive channels. Four subarrays are fabricated in a standard printed circuit board (PCB) process to investigate the planar dipole array antenna theoretically and experimentally. Both simulated and measured results show that the proposed array antenna achieves 87.0% impedance bandwidth (VSWR < 2.0 in the normal direction) from 1.3 GHz to 3.3 GHz, according to the specific requirements of an MPAR project. The active VSWR is less than 2.0 and 3.0 while the scan angle is $-30° \sim 30°$ and $-45° \sim 45°$, respectively. It means that this array antenna has wide-scan capability. In general, the balanced optimization between the electrical and mechanical performances makes the proposed array antenna attractive for MPARs and other compact systems.

1. INTRODUCTION

Multifunction phased array radars (MPAR) have an ability to perform multiple tasks simultaneously from the same platform [1–3]. This concept originated from an official research program to evaluate the feasibility of replacing traditional isolated civil radars in USA with a network of phased array radars (PAR). The application range of MPAR has been extended significantly to cover both military and civilian fields in recent years. In general, an MPAR can achieve all the functions that must be realized by multiple conventional radars with greater flexibility and lower cost. In MPAR, an ultra-wideband (UWB) array antenna has to be designed for ensuring the system multifunctionality. In the context of compact applications, the array antennas have difficulty balancing the electrical and mechanical performances. Besides their electrical performances, the volume and weight of such a UWB array antenna are also highly demanding, especially the low-profile feature. It is crucial for the airborne and spaceborne PARs because of limited payload capacity.

Several kinds of antenna structures designed for UWB applications have been proposed in recent years. Microstrip patch antennas are attractive solutions due to their advantages of low profile, light weight, and convenient integration with active circuits and components [4]. Many broadband techniques have been investigated to improve the inherent bandwidth of microstrip patch antennas [5–8]. Note that the bandwidth still limits their applications in some cases. Conversely, printed monopole antennas have larger impedance bandwidth than microstrip patch antennas [9–11]. However, these kinds of antenna structures are not in low profile due to the metallic ground planes perpendicular to the radiation elements. It can be concluded that the balance between the low-profile and UWB characteristics is important for MPAR applications, neither can be neglected. According to this requirement, planar

dipole antenna [12–15] is preferred as a possible improved solution. Low-profile and UWB characteristics can be achieved based on the coplanar feeding structures. However, these antennas are not designed specifically for array applications. The antenna structures should be miniaturized and optimized to guarantee good performances of the array antenna, such as active VSWR and radiation patterns.

In this study, a UWB array antenna with low profile is proposed for MPAR applications. The planar dipoles with large bandwidth are utilized to constitute the array antenna. A microstrip-sector feeding mechanism and reflecting ground plane are adopted to improve the radiation pattern. A prototype of a 64-element antenna array is fabricated to verify the performances through simulations and experiments. The remainder of this article is organized as follows. Section 2 introduces the structures of planar dipole element and the architecture of array antenna. Section 3 describes and discusses the simulated and measured results in detail. Finally, Section 4 concludes the article with highlights on the balanced optimization between electrical and mechanical performances of the proposed array antenna.

2. ARRAY ANTENNA DESIGN

The first step of array antenna design is to achieve an array element model with good performances. Fig. 1 shows the geometry of the planar dipole antenna with detailed dimensions. The antenna is composed of four parts: a pair of elliptical radiation patches with major axes a and minor axes b, a microstrip-sector feeding structure, a metallic ground plane, and a vertical coaxial feed. The radiation patches and the feeding structure are etched on the lower and upper surfaces of the substrate, respectively. The substrate has a relative dielectric constant ε_r of 2.65 with thickness h_1. A microstrip-sector feeding structure is employed to excite the radiation patches through a wideband unbalance-to-balance transition. It is composed of a $50\,\Omega$ microstrip transmission line of width w and a sector strip of radius r and angle θ. The metallic ground plane is fabricated below the foam substrate ($\varepsilon_r = 1.05$) with thickness h_2. The coaxial feed acts as a vertical transition from the SSMA connectors mounted on the metallic ground plane to the microstrip-sector feeding structure. This is the transmission path of radio frequency (RF) power. Hence, the power can be fed into the coupling slot between radiation patches through non-contact mode. It makes the radiation patterns insensitive to the feeding position.

Detailed parameters of the planar dipole antenna which acts as an array element are provided in Table 1. The operation frequency is mainly determined by the major axes and minor axes of radiation
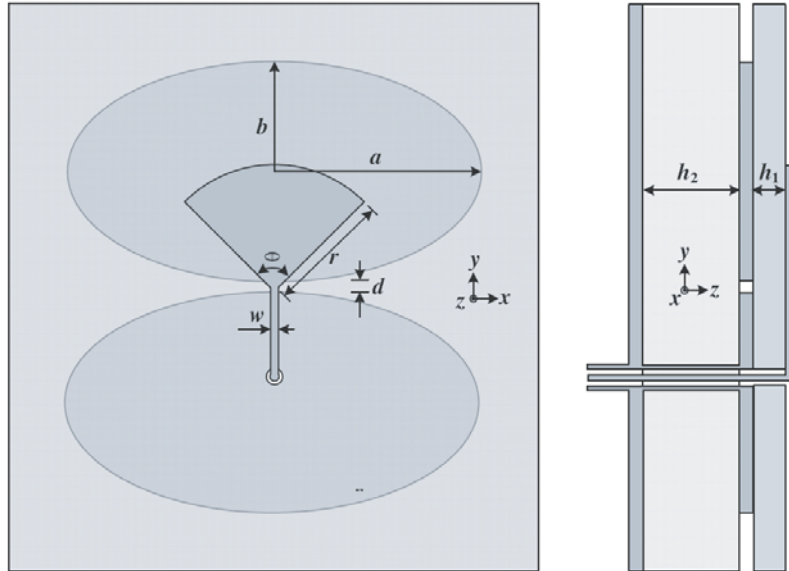

Figure 1. Geometry of the planar dipole antenna which acts as an array element. (a) Front view. (b) Side view.

patches. The relation between these parameters can be evaluated empirically by

$$f_0 \approx \frac{300}{2\,(a + 4b)} \tag{1}$$

where f_0 is the central frequency. Based on the parameters listed in Table 1, the value of f_0 is estimated at 2.0 GHz. The gap distance d between radiation patches is directly related to the impedance matching of the dipole. This is related to the coupling efficient when the RF power is coupled from the microstrip-sector feeding structure to the radiation patches. Hence, it is the key parameter which determines the operating bandwidth of the planar dipole antennas in the optimization procedure.

Table 1. Parameters of the planar dipole antenna.

Parameters	Parameters of the planar dipole antenna							
	a	b	d	w	h_1	h_2	r	θ^*
Values	28	12	0.8	1.345	0.25	19	14	90

* This unit is degree, the others are mm.

Due to low-profile and UWB characteristics, the planar dipole elements are utilized to constitute a subarray antenna with 16-element (4×4). Fig. 2 shows the layout of the subarray antenna, where dx and dy are the horizontal (x-axis) and vertical (y-axis) spacings, respectively. According to the principle of phased array antenna, the scan capability of the array antenna is determined by the element spacing. The allowable element spacing without grating lobe can be written as [16]

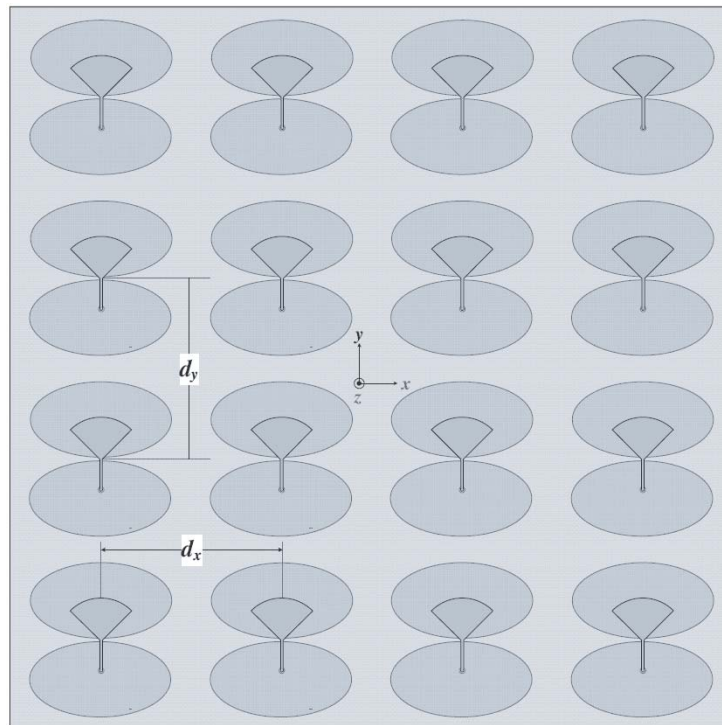$$d < \frac{\lambda}{1 + |\sin \theta_{\max}|} \tag{2}$$

Figure 2. Layout of the 16-element (4×4) subarray antenna The element spacing $dx = dy = 60$ mm.

where λ is the wavelength, and $\theta_{\max}$ is the maximum scan angle. The maximum element spacing can be set as $dx = dy = 60\,\text{mm}$ when $\theta_{\max}$ is $30°$ at $3.3\,\text{GHz}$. The scan angle becomes larger at lower frequencies for certain element spacing. There are 16 coaxial feeding ports on the lower surface of the subarray. They can be fed by the transmit/receive (T/R) modules in an active phased array radar.

A prototype of 64-element array antenna is built to verify the electrical performances. Fig. 3 shows the radiation surface of the array antenna. The ginkgo leaf shape on the radiation surface is the microstrip-sector feeding structure. The profile of the prototype is about $19.3\,\text{mm}$, which is equivalent to 8.4% of the wavelength at $1.3\,\text{GHz}$. It is much thinner than the conventional array antennas, such as Vivaldi antenna [17] and monopole antenna. Based on the low-profile array antenna, the MPAR designer can achieve an advanced solution known as the tiled array antenna [18]. In such a solution, the MPAR has compact volume and light weight by using a layered architecture. It is beneficial for realizing a large antenna aperture in the MPAR. The total weight of the prototype is $0.57\,\text{kg}$, which corresponds to the surface density $2.47\,\text{kg/m}^2$. The light-weight feature makes the proposed array antenna attractive for the airborne and spaceborne MPAR.

Figure 3. Photo of the prototype of 64-element antenna array. The profile of the array antenna is about $19.3\,\text{mm}$.

3. ARRAY ANTENNA PERFORMANCES

The simulation of the array antenna with periodic boundary condition is accomplished in the Ansys HFSS [19], which is a finite element method (FEM) based simulator [20] for electromagnetic structures. The master/slave boundaries are set in the simulation for extending an infinite array antenna from a planar dipole element. The scan capability of the array antenna can be investigated by changing the scan angle. Fig. 4 shows the simulated voltage standing wave ratio (VSWR) versus frequency when the array antenna scans in the E-plane (Fig. 4(a)) and H-plane (Fig. 4(b)). Four curves in the figure denote different scan angles of $0°$, $15°$, $30°$, and $45°$, respectively. It can be observed that the active VSWR in the frequency range $1.3 \sim 3.3\,\text{GHz}$ is better than 2.1 when the scan angle is swept from $-30°$ to $30°$. If the maximum scan angle is increased to $45°$, the active VSWR deteriorates slightly to 2.5. It means that the proposed array antenna has UWB wide-scan performances.

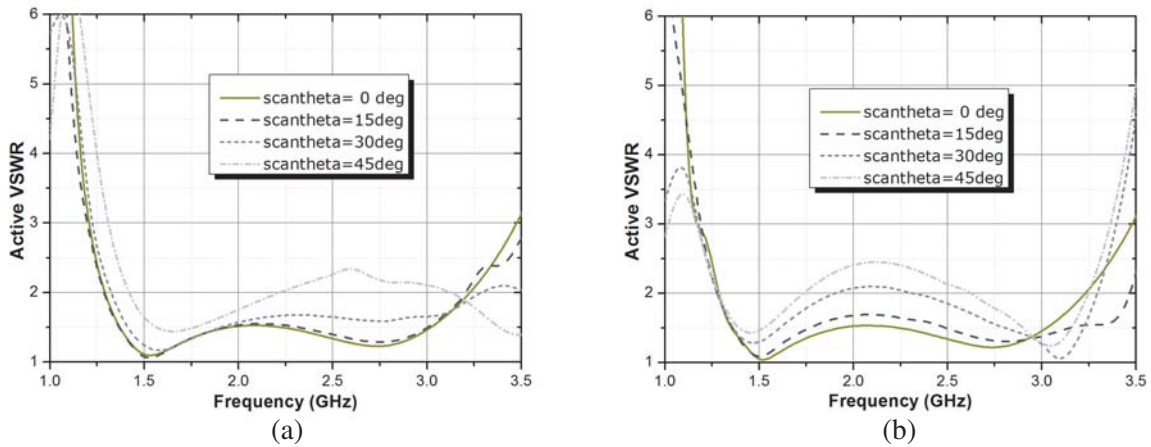The beamwidth of the antenna element is another factor related with the scan capability of the

Figure 4. Simulated active VSWR when the array antenna scans in (a) E-plane, and (b) H-plane.
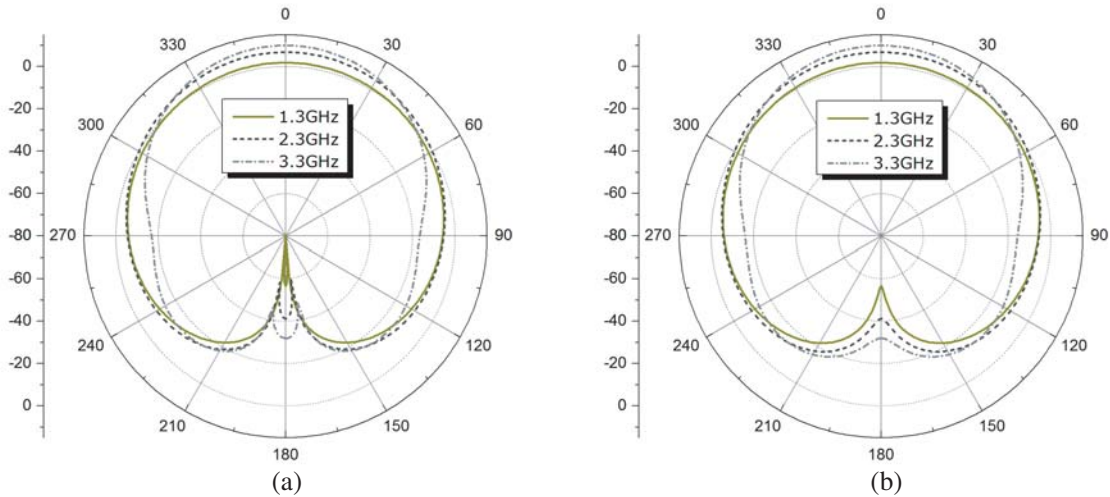

Figure 5. Simulated radiation patterns of the antenna element at 1.3, 2.3, and 3.3 GHz in (a) E-plane, (b) and H-plane.

array antenna. Fig. 5 shows the simulated radiation patterns of the antenna element in the periodic boundary condition. Patterns in the E-plane and H-plane are illustrated in Figs. 5(a) and (b), respectively. Three curves denote different frequencies of 1.3, 2.3, and 3.3 GHz. It can be observed that the radiation patterns in different cross sections are similar except the backward radiation. The symmetry of radiation patterns in bandwidth concludes that the microstrip-sector feeding mechanism has little negative influence upon the radiation of planar patches. Hence, this feeding mechanism has UWB characteristics. The beamwidth of radiation patterns for 1.3, 2.3, and 3.3 GHz are 105.8°, 74.2°, and 57.6°, respectively. It is inversely proportional to the effective aperture at different frequencies. For a certain physical aperture, the effective aperture is increased with the frequency. Simulated beamwidth shows that the array antenna is capable of scanning $-45° \sim 45°$ at 1.3 GHz and $-25° \sim 25°$ at 3.3 GHz.

The prototype of the 64-element array antenna is also investigated experimentally. The concept of active VSWR denotes the impedance matching of a finite array for different scan angles. It can be measured by using an equivalent method according to the mutual coupling between elements in an array [21]. The functional diagram of the measuring method is shown in Fig. 6. The coupling coefficients between the element under test and the other elements can be obtained. In the measurement, the element under test is connected to one port of the network analyser. The other port of the network

analyser should slide to the next element until all the adjacent elements have been measured. According to engineering experiences, the array prototype designed for evaluating the scan capability should be more than 5×5 elements. The centre element in the prototype is usually selected as the element under test.

Assuming an array antenna with $M \times N$ elements shown in Fig. 6, the reflection coefficient of the centre element is written on the basis of the coupling coefficients

$$\Gamma_{mn}(\theta_0, \varphi_0) \approx \sum_{p=1}^{M} \sum_{q=1}^{N} \{S_{mn,pq} \exp\left[-j(p-m)kd_x \sin\theta_0 \cos\varphi_0\right] \cdot \exp\left[-j(q-n)kd_y \sin\theta_0 \sin\varphi_0\right]\} \tag{3}$$

where $S_{mn,pq}$ is the coupling coefficients between the centre element (m, n) and the adjacent element (p, q); (θ_0, φ_0) is the beam direction of the array antenna; k is the wave number at measuring frequency; d_x and d_y are the element spacing in the x-axis and y-axis, respectively. In the prototype of the 64-element array antenna shown in Fig. 3, the centre element is denoted as a number of $(4, 4)$. In the measurement, the active VSWR $= (1+\Gamma)/(1-\Gamma)$ can be determined directly according to Eq. (3) when the coupling matrix between adjacent elements is measured.
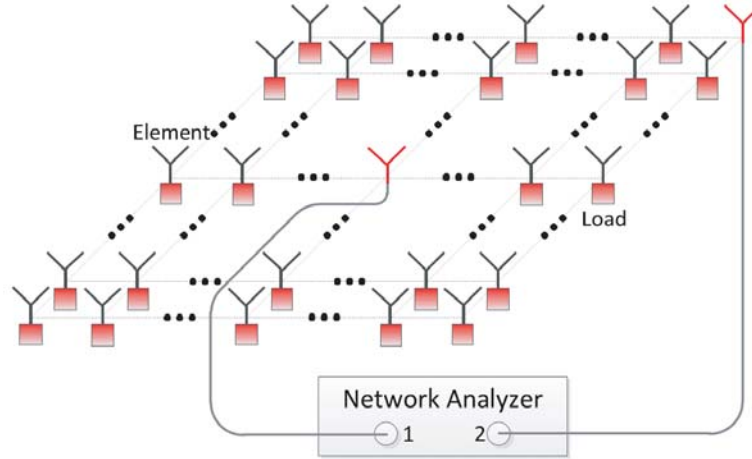

Figure 6. Functional diagram of the measuring method for the active VSWR of the centre element in an array antenna.

Figure 7 illustrates the measured active VSWR of the element under test (i.e., the centre element) in the prototype of 64-element array antenna for different scan angles. All the simulated results shown in Fig. 4 are evaluated again in experiments. It can be seen that the measured VSWR is in qualitative consistent with the simulated results. The slight difference between these two results is caused by different array configurations in the measurement and simulation. The infinite array and periodic boundary condition are assumed for the simulation. It is different from the finite array demonstrated in the measurement. In conclusion, the consistence between the simulated and measured results shows that the array prototype with 8×8 elements is suitable for the performance demonstration.

Radiation patterns of the array prototype are measured by using the planar near-field scanning technique. Fig. 8 illustrates the measured radiation patterns in E-plane and H-plane. The radiation performances at 1.3 GHz, 2.3 GHz, and 3.3 GHz are evaluated in an anechoic chamber. Measured results show that the main beam is narrowed with the frequency. It is because the effective aperture of the array antenna becomes larger at higher frequencies. As with the single antenna element, rotational symmetrical main-beams are achieved in the measured patterns of the array antenna. This is mainly due to the employment of the microstrip-sector feeding mechanism, which is harmless to the structural symmetry of planar dipole antenna. Therefore, the proposed array antenna is similar to the conventional dipole antennas in radiation patterns, but with much better mechanical performances.
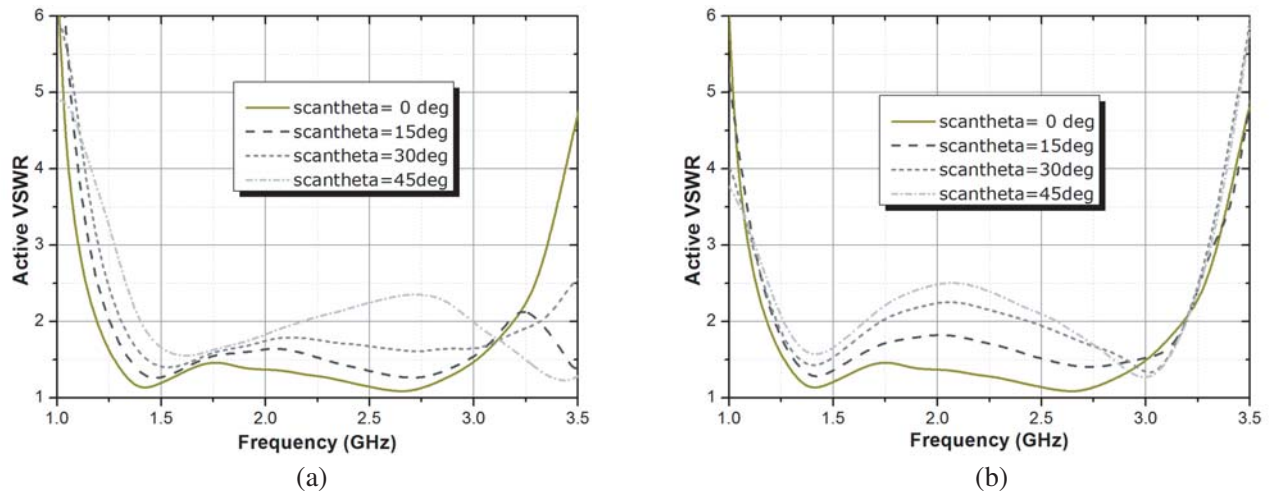
Figure 7. Measured active VSWR when the array antenna scans in (a) E-plane, and (b) H-plane.
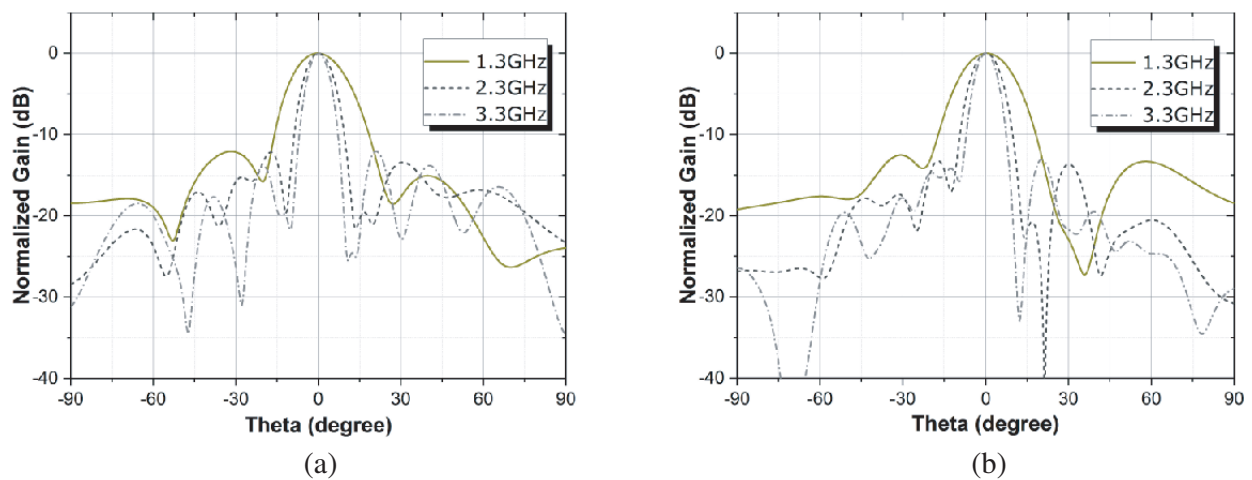

Figure 8. Measured radiation patterns of the array prototype at 1.3, 2.3 and 3.3 GHz in (a) E-plane, and (b) H-plane.

4. CONCLUSIONS

The application range of MPARs has been extended significantly in the civil and military fields. A UWB array antenna with low profile is required for the design of MPAR. Therefore, the planar dipole array is presented in our study. An optimized feeding mechanism with microstrip-sector is adopted to maintain the structural symmetry of the array antenna. So similar radiation patterns can be obtained in E-plane and H-plane. The prototype of 64-element array antenna is investigated in simulations and measurements. Both simulated and measured results show that the proposed array antenna achieves good impedance matching over the frequency range from 1.3 to 3.3 GHz. In addition, the profile of the array antenna is less than one-tenth of the wavelength at the lower frequency. It means that both the low-profile and UWB characteristics can be obtained based on the proposed array antenna.

REFERENCES

1. Stailey, J. E. and K. D. Hondl, "Multifunction phased array radar for aircraft and weather surveillance," *Proceedings of the IEEE*, Vol. 104, No. 3, 649–659, 2016.

2. Herd, J., S. Duffy, M. Weber, et al., "Advanced architecture for a low cost multifunction phased array radar," *IEEE MTT-S Int. Microw. Symp.*, 676–679, Anaheim, USA, May 2010.

3. Herd, J., S. Duffy, D. Carlson, et al., "Low cost multifunction phased array radar concept," *IEEE Int. Symp. on Phased Array Systems and Tech.*, 457–460, Waltham, USA, October 2010.

4. Kumar, G. and K. P. Ray, *Broadband Microstrip Antennas*, Artech House, Dedham, USA, 2003.

5. Chen, Z. N. and M. Y. W. Chia, "Center-fed microstrip patch antenna," *IEEE Trans. on Antennas and Propag.*, Vol. 51, No. 3, 483–487, 2003.

6. Koohestani, M. and M. Golpour, "U-shaped microstrip patch antenna with novel parasitic tuning stubs for ultra wideband applications," *IET Microw. Antennas Propag.*, Vol. 4, No. 7, 938–946, 2010.

7. Donelli, M. and P. Febvre, "An inexpensive reconfigurable planar array for Wi-Fi applications," *Progress In Electromagnetics Research C*, Vol. 28, 71–81, 2012.

8. Moriyama, T., M. Manekiya, and M. Donelli, "A compact switched-beam planar antenna array for wireless sensors operating at Wi-Fi band," *Progress In Electromagnetics Research C*, Vol. 83, 137–145, 2018.

9. Agrawall, N. P., G. Kumar, and K. P. Ray, "Wide-band planar monopole antennas', *IEEE Trans. Antennas Propag.*, Vol. 46, No. 2, 294–295, 1998.

10. Ammann, M. J. and Z. N. Chen, "Wideband monopole antennas for multi-band wireless systems," *IEEE Antennas Propag. Mag.*, Vol. 45, No. 2, 146–150, 2003.

11. Robol, F. and M. Donelli, "Circularly polarized monopole hook antenna for ISM-band systems," *Microw. and Optical Tech. Lett.*, Vol. 60, No. 6, 1452–1454, 2018.

12. Schantz, H. G., "Planar elliptical element ultra-wideband dipole antennas," *IEEE Antennas Propag. Society Int. Symp.*, 44–47, Boston, USA, June 2002.

13. Schantz, H. G., "Bottom fed planar elliptical UWB antennas," *IEEE Ultra Wideband Syst. Tech. Conf.*, 219–223, Virginia, USA, November 2003.

14. Zhang, J. P., Y. S. Xu, and W. D. Wang, "Ultra-wideband microstrip-fed planar elliptical dipole antenna," *Electron. Lett.*, Vol. 42, No. 2, 144–145, 2006.

15. Li, B., J. P. Zhang, Y. Deng, et al., "Design of a low-profile ultra-wideband antenna array based on planar dipole elements," *2018 IEEE Radar Conference*, 385–388, Oklahoma, USA, April 2018.

16. Zhang, G. Y. and Y. J. Zhao, *Technologies of Phased Array Radar*, Publishing House of Electronics Industry, Beijing, China, 2006.

17. Stockbroeckx, B. and A. V. Vorst, "Copolar and cross-polar radiation of Vivaldi antenna on dielectric substrate," *IEEE Trans. on Antennas and Propag.*, Vol. 48, No. 1, 19–24, 2000.

18. Lyon, R. W., A. M. Kinghorn, G. D. Morrison, et al., "Active electronically scanned tiled array antenna," *IEEE Int. Symp. on Phased Array Systems and Tech.*, 160–165, Boston, USA, October 2013.

19. HFSS Introduction, http://www.ansys.com/products/electronics/ansys-hfss, accessed 1 January 2019.

20. Dhatt, G., G. Touzot, and E. Lefrancois, *Finite Element Method*, John Wiley & Sons, New York, 2012.

21. Gross, F. B., *Frontiers in Antennas: Next Generation Design and Engineering*, McGraw-Hill, New York, USA, 2011.